INSTITUT DE FRANCE
Académie des sciences

Comptes Rendus

Géoscience

Sciences de la Planète

Jérémie Aubineau, Olabode M. Bankole, Fabien Baron, Brian Grégoire and Abderrazak El Albani

Authigenic kaolinite and sudoite in sandstones from the Paleoproterozoic Franceville sub-basin (Gabon)

Volume 353, issue 1 (2021), p. 209-226

Published online: 5 July 2021

https://doi.org/10.5802/crgeos.62

Les Comptes Rendus. Géoscience — Sciences de la Planète *sont membres du Centre Mersenne pour l'édition scientifique ouverte*
www.centre-mersenne.org
e-ISSN : 1778-7025

Comptes Rendus
Géoscience — Sciences de la Planète
2021, 353, nº 1, p. 209-226
https://doi.org/10.5802/crgeos.62

Review Article — Petrology, Geochemistry

Authigenic kaolinite and sudoite in sandstones from the Paleoproterozoic Franceville sub-basin (Gabon)

Jérémie Aubineau *, [a, b], **Olabode M. Bankole** [b], **Fabien Baron** [b], **Brian Grégoire** [b] **and Abderrazak El Albani** [b]

[a] Géosciences Montpellier, UMR 5243, CC 60 – University of Montpellier, Montpellier, France

[b] IC2MP UMR 7285 CNRS, University of Poitiers, Poitiers, France

E-mails: jeremie.aubineau@umontpellier.fr (J. Aubineau), olabode.bankole@univ-poitiers.fr (O. M. Bankole), fabien.baron@univ-poitiers.fr (F. Baron), brian.gregoire@univ-poitiers.fr (B. Grégoire), abder.albani@univ-poitiers.fr (A. El Albani)

Abstract. The mineral paragenetic sequence of the 2.1-billion-year-old (Ga) Francevillian basin is important for understanding the diagenetic fluid history that allowed the preservation of the oldest ecosystem, including bacterial and more advanced forms of life in the FB_2 Member. However, a full characterization of the clay mineralogy of the FB_2 microbial mat-related structures (MRS) and associated host sediments (sandstones and black shales) is yet to be determined. Petrographic, microscopic, and mineralogical analyses reveal the concurrent presence of authigenic vermiform kaolinite and sudoite in the MRS and host sediments. Kaolinite formed along cleavages of altered muscovite and as pore-filling during early diagenesis, while sudoite likely precipitated at the expense of kaolinite that undergone secondary dissolution later in the diagenetic sequence. The formation of sudoite was promoted by fault-controlled acidic and oxidized brines that might have migrated during the Francevillian basin inversion. These results imply that the porosity and permeability of sedimentary rocks dominantly control the mineralogical assemblage of the FB_2 Member.

Keywords. Sudoite, Kaolinite, Diagenesi, Paragenesis, Sandstones, Franceville sub-basin.
Manuscript received 21st March 2021, revised and accepted 1st June 2021.

1. Introduction

Sudoite is characterized by a dioctahedral 2:1 layer and a trioctahedral interlayer sheet and belongs to the di-trioctahedral chlorite mineral group with an ideal composition of $(Al_3Mg_2)(Si_3Al)O_{10}(OH)_8$ [Bailey, 1980]. Although this type of Al- and Mg-rich chlorite is far less common than its tri-trioctahedral Mg- and Fe-rich countertype, sudoite usually occurs in low-temperature environments [<300 °C; Beaufort et al., 2015, Lanari et al., 2014], including diagenetic and hydrothermal systems [e.g., Beaufort et al., 2005, Daniels and Altaner, 1990, Hayashi and Oinuma, 1964, Hillier et al., 2006, Percival and Kodama, 1989, Rodríguez-Ruiz et al., 2019, Ruiz Cruz and Sanz de Galdeano, 2005, Schultz, 1963, Truche et al., 2018]. In such geological settings, sudoite likely forms from modifications of kaolin minerals (i.e., kaolinite, dick-

* Corresponding author.

ite, and nacrite) through a stepwise reaction under the influence of Mg-rich fluids. Sudoite also crystallizes at the expense of diagenetic beidellite when kaolins are lacking [Biernacka, 2014]. These mineral transformations are generally controlled by a dissolution–crystallization mechanism since convincing evidence of kaolinite–sudoite or smectite–sudoite mixed-layer minerals (MLMs) are lacking [see review in Beaufort et al., 2015]. A large amount of sudoite has been reported in the Proterozoic uranium (U)-bearing sandstones that unconformably overlie Archean basements [Beaufort et al., 2005, Billault et al., 2002, Kister et al., 2005, Percival and Kodama, 1989, Riegler et al., 2014, Truche et al., 2018], where the origin of sudoite was believed to have resulted from interactions of oxidized and acidic fluids with the underlying crystalline rocks within active fault zones. Therefore, sudoite can sometimes be a potential proxy for tracing U mineralization.

Despite numerous studies on the diagenetic mineral phases of the Paleoproterozoic Franceville subbasin of Gabon [Aubineau et al., 2019, Bankole et al., 2018, 2016, 2015, Bros et al., 1992, Gauthier-Lafaye, 1986, Ngombi-Pemba et al., 2014, Ossa Ossa et al., 2013, Weber, 1968], the presence of kaolin minerals and di-trioctahedral chlorite have not been well-documented or constrained in the Francevillian rock sequence, especially in sandstones [cf. Ngombi-Pemba et al., 2014]. Synthetically, assemblages of detrital-shaped (including mica and ferromagnesian chlorite) and diagenetic (illite, tri-trioctahedral chlorite, and smectite-rich and illite-rich illite–smectite, I-S MLMs) clay minerals dominantly characterize the Francevillian Group sedimentary rocks. Most of the diagenetic clay minerals in the Francevillian sediments result from the alteration of aluminosilicate minerals [Gauthier-Lafaye, 1986]. The surprising survival of smectite-rich (R0) I-S MLMs in localized stratigraphic levels (from the FB_{1b}, to the FB_{2b} units) of the Franceville sub-basin has been attributed to potassium deficiency in the system [Aubineau et al., 2019, Bankole et al., 2015, Ngombi-Pemba et al., 2014]. Indeed the variable proportion of K-feldspar was recognized in other rock units of the Franceville sub-basin [Bankole et al., 2015, Ngombi-Pemba et al., 2014], suggesting mixing of multiple source rocks [Bankole et al., 2020].

The FB_2 Member of the Franceville sub-basin is believed to host the earliest potential multicellular life [El Albani et al., 2014, 2010] capable of movement [El Albani et al., 2019] and has provided a considerable interest in the complex life's early evolution. Thus, deciphering the post-depositional modification processes in these unmetamorphosed sedimentary rocks may provide a glimpse of long-term effects of diagenetic history on the preservation of the Francevillian biota. This paper investigates the di-trioctahedral chlorite and kaolin minerals in sandstone and black shale facies of the Francevillian FB_2 Member. Here we integrated X-ray diffraction (XRD), infrared spectroscopy, and optical and electron microscopy to examine the clay mineralogy and petrography of authigenic minerals and their textural relationships to provide additional insights into the diagenetic fluid history and mineral paragenetic sequence in the Franceville sub-basin of the Francevillian Group.

2. Geological setting

The Francevillian basin is composed of four intracratonic sub-basins—Booué, Lastourville, Okondja, and Franceville—in southeastern Gabon [Bouton et al., 2009]. The basin fill consists of 1.0 to 2.5-km-thick Paleoproterozoic siliciclastic sedimentary succession commonly referred to as the Francevillian Group [Figure 1a; Weber, 1968]. Importantly, the Francevillian deposits were not affected by metamorphic processes and have only been subjected to diagenetic and low-temperature hydrothermal processes [Aubineau et al., 2020, Bankole et al., 2016, 2015, Gauthier-Lafaye and Weber, 1989]. Specifically, the Franceville sub-basin records a maximum burial depth and temperature of about 2500 m and 80 °C, respectively [Ngombi-Pemba et al., 2014, Weber, 1968], which corresponds to burial conditions of a common geothermal gradient.

These sediments rest unconformably on the Archean crystalline basement within the west Congolese craton. The basement rocks are mainly composed of Mesoarchean (3200–2800 Ma), TTG (tonalite–trondhjemite–granodiorite), and greenstone belts [Mouélé et al., 2014, Thiéblemont et al., 2009]. The synthesis of the geodynamic evolution of the Francevillian basin was recently detailed by Weber et al. [2016].

The Francevillian Group has been divided into five lithostratigraphic formations, labeled FA to FE

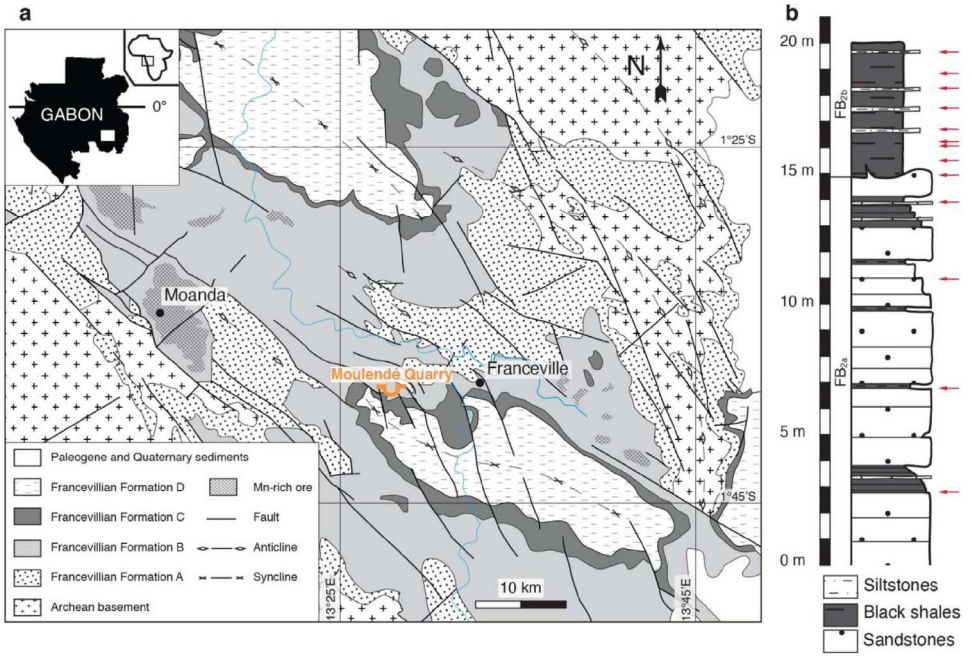

Figure 1. (a) Geological map of the Paleoproterozoic Franceville sub-basin showing the study area—Moulendé Quarry [modified from Bouton et al., 2009]. (b) Lithostratigraphic column of the FB_2 Member in the Moulendé Quarry displaying sampling positions of both microbial mat structures and host sediments (red arrows). Images in (a) and (b) are modified from Aubineau et al. [2020] and Aubineau et al. [2019], respectively.

from the oldest to the youngest. The Lower FA formation is dominated by braided fluvial conglomerates and sandstones, while the Upper FA formation is composed of fluvio-deltaic, fine-grained mudstones and sandstones [Bankole et al., 2015, Feybesse et al., 1998, Gauthier-Lafaye and Weber, 1989]. This sedimentation occurred during a progressive basin opening. The topmost part of the FA formation is marked by post-depositional formation of U ore deposits in association with bitumen [Bankole et al., 2016, Gauthier-Lafaye and Weber, 2003, 1989]. The overlying marine FB formation deposited during a period of tectonic subsidence and basin deepening is subdivided based on the lithostratigraphy into FB_1 (including a, b, and c units) and FB_2 (a and b units) members based on lithological differences and sedimentary structures [Azziley Azzibrouck, 1986, Weber, 1968]. The FB_1 Member deposited during sea-level rise is mainly characterized by greenish shales (FB_{1a} unit), rhythmic successions of greyish shale and dolomite-cemented siltstones (FB_{1b} unit), and manganese-rich black shales [FB_{1c} unit; Azziley Azzibrouck, 1986, Gauthier-Lafaye and Weber, 2003, Pombo, 2004, Reynaud et al., 2017]. Following an episode of sea-level fall, massive sandstones frequently intercalated by dm-thick black shale layers (FB_{2a} unit) that are capped by laminated black shales with interbedded siltstones (FB_{2b} unit) were deposited [Figure 1b; Reynaud et al., 2017]. In addition, the FB_2 Member sandstones and black shales host light-dependent, microbial mat morphotypes [Aubineau et al., 2021, 2019, 2018], previously described as pyritized mat-related structures (MRS) and non-pyritized MRS. These delicate MRS are closely associated with the well-preserved complex forms of life in the FB_{2b} unit [Aubineau et al., 2018, El Albani et al., 2019]. The overlying FC formation consists of shallow marine deposits of massive dolostones and cyanobacteria-hosting stromatolitic cherts with intercalation of black shale beds [Bertrand-Sarfati and Potin, 1994, Lekele Baghekema et al., 2017, Préat et al., 2011]. The FD formation

is composed of transgressive marine black shales with interbedded volcanic tuffs [Thiéblemont et al., 2014], while the uppermost FE formation contains arkosic sandstones and forms lenticular outcrops in the Okondja sub-basin [Gauthier-Lafaye and Weber, 1989, Thiéblemont et al., 2014]. Additionally, extensive descriptions and discussions of petrography, depositional facies, and stratigraphic and sedimentary evolution of the Lower Francevillian Group are provided in Bankole et al. [2016, 2015], Gauthier-Lafaye and Weber [2003, 1989] and Reynaud et al. [2017].

Despite numerous attempts to resolve the age and duration of deposition of the Francevillian Group [Bonhomme et al., 1982, Bros et al., 1992, Sawaki et al., 2017], the depositional age of siliciclastic sequence remains poorly constrained. U–Pb ages of 2083 ± 6 Ma and 2072 ± 29 Ma were reported from tuffs and epiclastic sandstones in the FD formation, respectively [Horie et al., 2005, Thiéblemont et al., 2009]. In addition, the FB and FC formations have recorded extremely positive $\delta^{13}C$ values in marine carbonates [El Albani et al., 2010, Préat et al., 2011], which are thought to correspond to the end of the longest-lived positive carbon isotope excursion in Earth's history [i.e., Lomagundi event, 2.22–2.06 Ga; Karhu and Holland, 1996]. Collectively, these age constraints place the age of deposition for the Francevillian Group close to ca. 2.15–2.08 Ga [Canfield et al., 2013].

3. Samples and analytical techniques

3.1. *Sampling*

Heterogeneous microbial mat morphotypes (both pyritized and non-pyritized MRS, defined from their petrographic and geochemical analyses, Aubineau et al., 2018), and their host sandstone and black shale sediments were collected from outcrops in the Moulendé Quarry (Figure 1b). The weathered outermost surfaces were removed before sampling outcrop sediments. We carefully separated the µm-thick mat laminae from underlying sediments with a stainless-steel razor blade, avoiding as much as possible contamination with the underlying host rocks. The host sediments were directly extracted below the MRS with a hammer.

3.2. *X-ray diffraction (XRD)*

The <2 µm clay fraction of MRS and host sediment samples were analyzed with a Bruker D8 ADVANCE diffractometer at the University of Poitiers using a CuKα radiation, operating at 40 kV and 40 mA. The dispersion of gently hand-crushed bulk samples in deionized water with an Elma S60 ultrasonic agitation device without any chemical pre-treatment [Moore and Reynolds Jr., 1997] allowed the extraction of the <2 µm clay fraction by sedimentation. Oriented preparations of the <2 µm size fraction were prepared by drying ~1 mL of suspension on glass slides at room temperature. The oriented mounts were examined at a step size of 0.02° 2θ using a 3 s counting time per step and recorded from a 2–30° 2θ angular range after successive air-dried (AD) and ethylene glycol (EG) saturation. In addition, the octahedral occupancy within chlorite minerals was measured based on the peak position of the 060 reflection on randomly oriented <2 µm clay fraction over a 57–63° 2θ angular range with a step size of 0.025° 2θ per 8 s counting time. Bruker Eva software was used for background stripping, indexing of XRD peaks and mineral identification by comparing with International Centre for Diffraction Data (ICDD) files.

The NEWMOD 2.0 program was used to semi-quantitatively estimate the relative clay proportions in the <2 µm fractions by fitting experimental samples in AD and EG states [Reynolds Jr. and Reynolds III, 1996]. We introduced the instrumental and experimental factors, including the divergence slit, goniometer radius, soller slits, sample length, and quartz reference intensity, which are specific to the Bruker D8 ADVANCE diffractometer. Sigmastar and the mass adsorption coefficient for Cu radiation were also set between 12 to 14° and 45 $cm^2 \cdot g^{-1}$, respectively [Moore and Reynolds Jr., 1997]. The XRD profile modeling is, however, difficult to apply on the low-angle region with the NEWMOD 2.0 program. The calculation of the fit does not include the non-clay mineral reflections.

3.3. *Microscopy*

Petrographic observation and documentation of textural relationships were made by optical and scanning electron microscopies at the University of Poitiers. Polished thin sections were first examined

under transmitted and reflected light using a Nikon ECLIPSE E600 POL microscope coupled with a Nikon Digital Sight DS-U1 camera and NIS-Elements D software. Carbon-coated rock slabs and thin sections were imaged with a JEOL JSM-IT500 scanning electron microscope (SEM) equipped with a Bruker energy-dispersive X-ray spectrometer (EDX). Investigations of the size and morphology of clay minerals in rock slabs were performed in secondary electron mode, while polished thin sections were studied in backscattered electron mode. Semi-quantitative analysis for mineralogical examination was carried out on C-coated polished rock slabs, using an FEI Quanta 200 SEM equipped with an EDX at the University of Lille. Analytical conditions of both SEM operated at an acceleration voltage of 10–15 kV, 1 nA beam current, and a working distance of 10.5 mm.

3.4. *Fourier transform infrared (FTIR) spectroscopy*

The bulk mineralogy and <2 μm clay fractions of MRS and host sediments were further analyzed by the FTIR spectroscopy at the University of Poitiers. Such analytical method is a powerful tool to distinguish the polymorph minerals of the kaolin group as well as the chlorite minerals by the examination of the fundamental hydroxyl-stretching vibrations in the 3800–3200 cm^{-1} region (middle infrared—MIR) of spectra. The samples were embedded in potassium bromide (KBr) pellets that consist of a mixture of 1 mg of sample and 149 mg of KBr, pressed for 5 min at 8 kbar, and dried overnight in an oven at 150 °C. MIR spectra were recorded in transmission mode from KBr pellets using a Nicolet iS50 FTIR spectrometer equipped with a KBr beamsplitter and a DTGS KBr detector. Each MIR spectrum corresponds to an accumulation of 100 scans at a resolution of 4 cm^{-1}.

4. Results

4.1. *Petrographic observation*

Petrographically, sandstones in the FB_{2a} unit dominantly consist of poorly sorted detrital quartz grains with minor clay and organic-rich matrix (Figure 2a, b). Elongated muscovite is sometimes bent at grain-to-grain contacts due to compaction and represents the dominant micaceous minerals. Concavo-convex features and stylolites between quartz grain contacts further characterize the compaction features. Although our observations were based on two-dimensional imaging methods, the primary porosity has been likely destroyed in the coarse-grained facies due to physical and chemical compaction effects. However, few intergranular pore spaces, mostly filled with organic matter and authigenic clay minerals, are sometimes preserved (Figure 2b). Petrographic observations also confirmed the absence of K-feldspars and the rare occurrence of plagioclase in the FB_{2a} sandstones, as previously described by Ngombi-Pemba et al. [2014]. Our petrological and mineralogical observations in the FB_{2b} black shales are similar and consistent with the detailed descriptions of Ngombi-Pemba et al. [2014].

The SEM–EDX examination reveals that the kaolin minerals commonly occur, filling secondary pores and replacements along the cleavage planes of altered muscovite in the FB_{2a} sandstones (Figure 2c, e, and f; Figures S1–S3). Kaolinization of muscovite is common in the studied coarse-grained samples. The consistent association between altered muscovite and kaolin minerals likely suggests the authigenic nature of the kaolin minerals. Kaolin aggregates typically form 5 to 10 μm-long, vermicular booklets composed of thin pseudohexagonal plates orderly stacked face to face (Figure 3a, b), which is consistent with the morphological features of kaolinite polymorph [Beaufort et al., 1998]. The individual platelets are homogeneous in size and morphology, with crystals of 5 μm wide and 0.1 μm thick. Importantly, kaolinite has undergone secondary dissolution (Figure 2f), as suggested by the partial dissolution of the edge of plates (Figure 3c).

SEM–EDX observations show that the ferromagnesian chlorite is present as either detrital particle or pore filling in the FB_{2a} sandstones (Figure 2d–f; Figures S1–S3), as suggested by the presence of O, Si, Al, Mg, and Fe elements. These clay morphologies are also found in the MRS at the top of the massive sandstones [Aubineau et al., 2019]. Authigenic Al- and Mg-rich chlorites are exclusively pore-filling and widely observed in the FB_{2a} sandstones but absent in the FB_{2b} black shales (Figure 2e, f; Figures S1–S3). At higher magnification, these diagenetic minerals consist of densely packed subhedral,

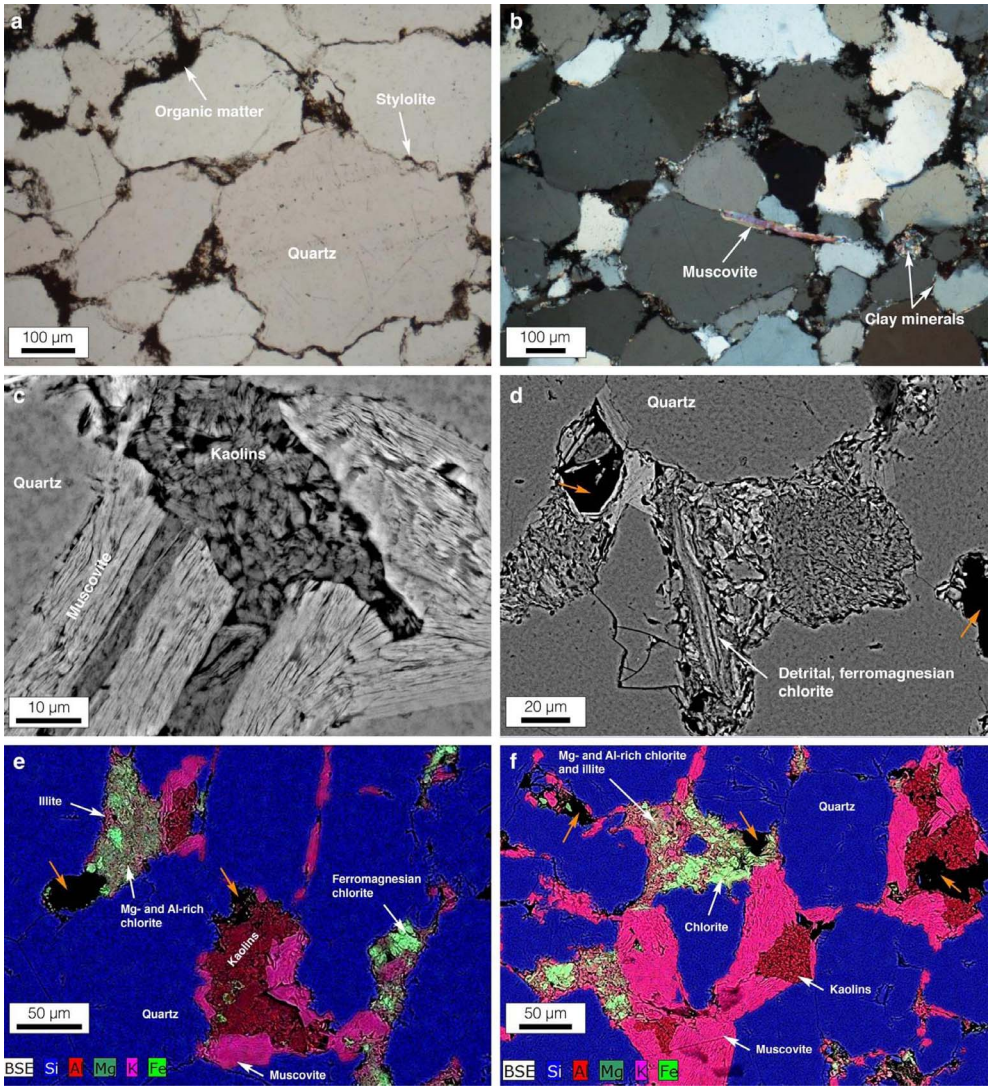

Figure 2. Optical and scanning electron microscope photomicrographs of the FB_{2a} sandstones. (a, b) Pore-filling organic matter and clay minerals in poorly sorted sandstones (PL and CP). The quartz grains experienced moderate to high degrees of compaction. (c) Authigenic pore-filling kaolin associated with altered detrital muscovite (BSE). (d) Detrital tri-trioctahedral chlorite. The presence of ferromagnesian chlorite is confirmed through the EDX spectrum in Figure S1a. (e, f) Elemental mapping showing the mineralogical composition of intragranular pores. EDX spectrum of sudoite is visible in Figure S1b. Composite elemental maps are displayed in Figures S2, S3. Orange arrows denote secondary pore spaces. PL: plane polarized, CP: cross polarized, BSE: back scattered electron.

folded, and platy <5 µm crystals (Figure 3d), forming a chaotic arrangement where flakes are perpendicular to the substratum surface (boxwork-like texture) and/or parallel to the wall-rock surface (parallel pattern). Such morphological features resemble those reported for sudoite [Billault et al., 2002].

4.2. *Mineralogy and chemical composition in the* FB_2 *Member*

The MRS, host sandstones, and black shales were analyzed using the XRD technique. Aubineau et al. [2019] pointed out the large contribution of illite-rich

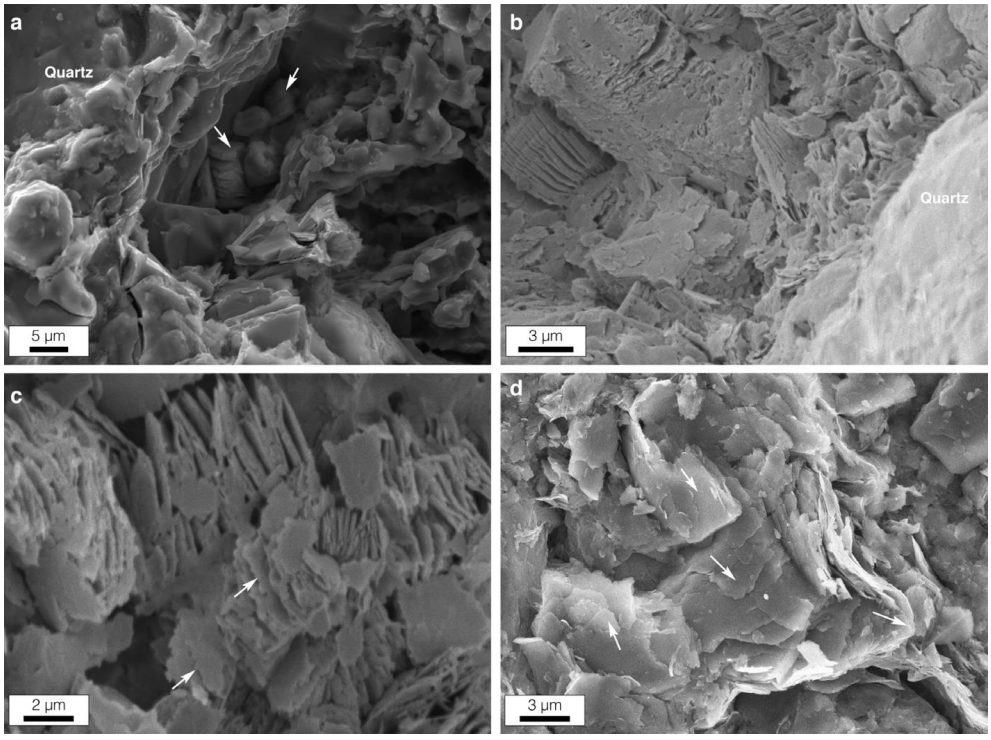

Figure 3. SEM images in secondary mode of pore-filling minerals from the FB_{2a} sandstones. (a, b) Authigenic vermiform crystals of kaolinite. (c) Partial dissolution of pseudohexagonal kaolinite (white arrows). (d) Mixture of boxwork-like texture and parallel pattern of sudoite crystals (white arrows). EDX spectrum of analysis points (arrows) is shown in Figure S1c.

(R3) I-S MLMs in the MRS (both non-pyritized and pyritized), while clay minerals in the underlying host sediments are enriched in R0 I-S MLMs. These assemblages contain both $1M_t$ and $2M_1$ illite polytypes in the FB_2 Member. Bulk mineralogy data show that the black shale facies have higher proportion of pyrite relative to sandstones, while dolomite is the dominant carbonate mineral in both lithologies [Aubineau et al., 2019].

The studied XRD profiles of oriented preparations of the <2 µm fraction in the AD state show characteristic 00*l* reflections of chlorite at ~14.2–14.1 Å, 7.1 Å, 4.72 Å, and 3.54 Å that remain unaffected after glycolation (Figure 4). There is no significant difference in the mineralogical composition of chlorite between the lithologies within the same rock unit, which suggests that the MRS did not affect the chlorite composition. The intensities of the 002 and 004 reflections of chlorites in the FB_{2b} unit are greater than the 003 reflection (Figure 4a), which is typical of tri-trioctahedral chlorite [Brindley and Brown, 1980]. In contrast, the high intensity of the 003 reflection of chlorite (Figure 4c) coupled with the 060 reflection at 1.51 Å (Figure 4d) indicate the presence of di-trioctahedral chlorite in the FB_{2a} unit [Billault et al., 2002]. The presence of 060 reflection at 1.55 Å also confirms the occurrence of tri-trioctahedral chlorite in the non-pyritized MRS and sandstones. Kaolinite in the FB_{2a} MRS and sandstones is characterized by the 001, 002, and 060 peaks at 7.15 Å, 3.57 Å, and 1.49 Å, respectively. The 00*l* kaolinite reflections are sharp and narrow, implying their well-crystallized phase.

The XRD profile modeling (NEWMOD program) confirm that sudoite is completely absent in the black shales but occasionally present in the sandstones and siltstones, reaching about 28% in the <2 µm clay fraction (Figure 5; Table S1). In contrast, variable abundances of chlorite without relationships with any clay minerals are observed in the FB_2 Member.

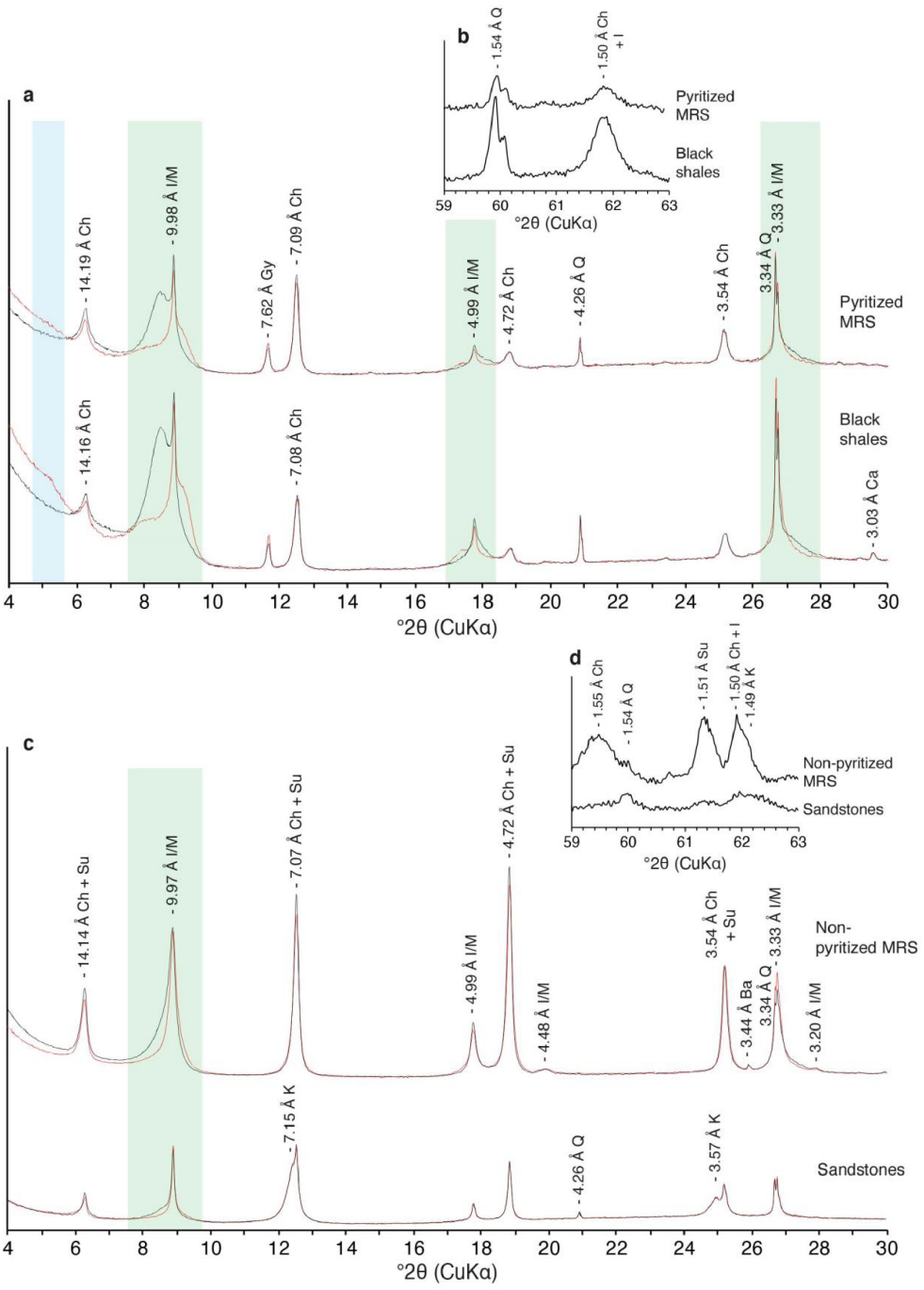

Figure 4. Representative XRD patterns of the <2 μm clay fraction of mat-related structures and host sediments in the FB_{2b} Member (a, b) and FB_{2a} Member (c, d). (a, c) Oriented preparations after air-drying (black lines) and glycolation (red lines). (b, d) XRD profiles of 060 reflection of randomly oriented preparations. The blue and green areas correspond to R0 I-S MLMs and R3 I-S MLMs, respectively, as previously described in Aubineau et al. [2019]; chlorite (Ch); illite/mica (I/M); gypsum (Gy); quartz (Q); calcite (Ca); sudoite (Su); barite (Ba); kaolinite (K).

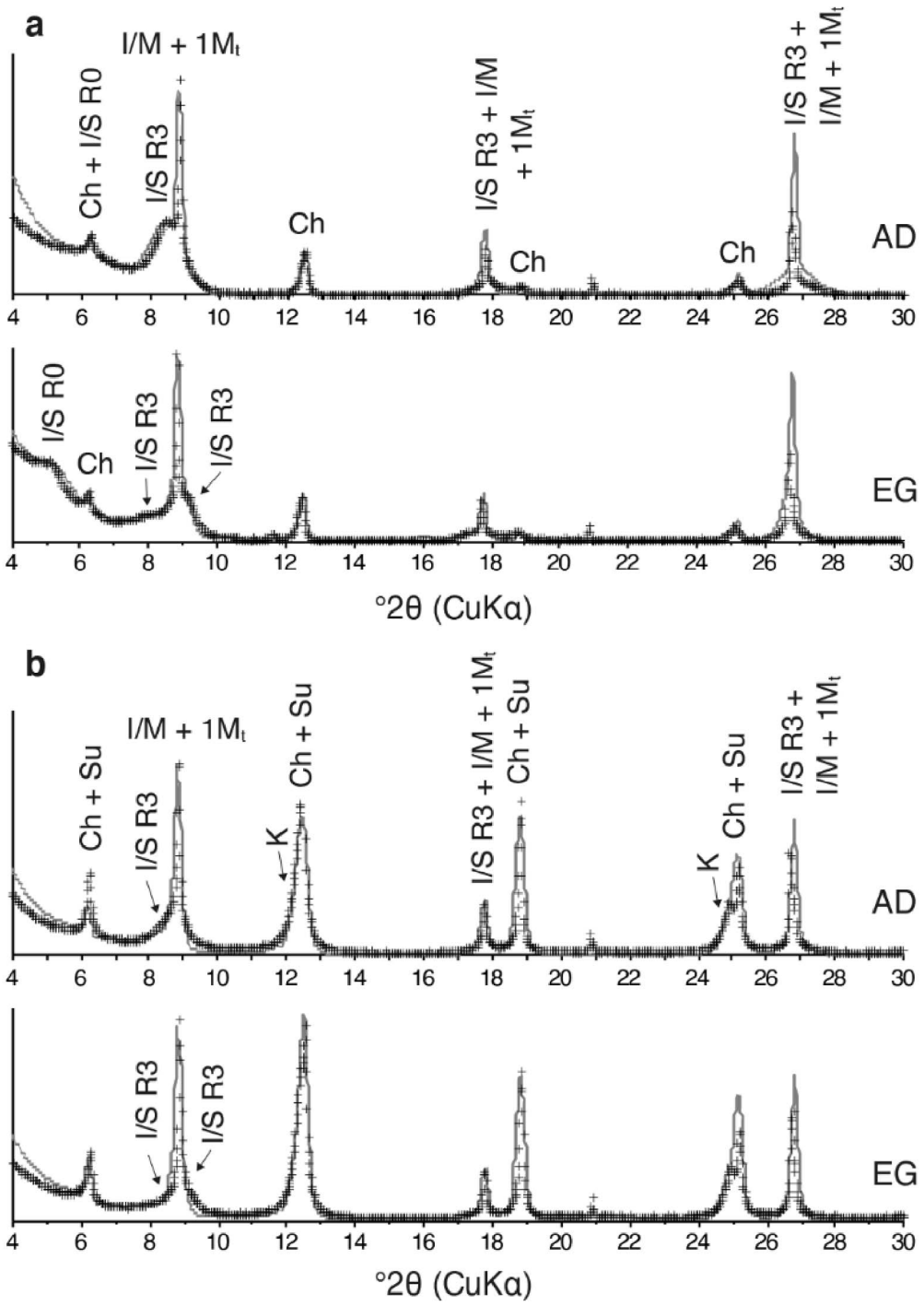

Figure 5. Experimental (crosses) and modeled (lines) XRD profiles of representative samples after air-dried (AD) preparation and ethylene glycol (EG) saturation. (a) Black shale. (b) Sandstone. (Chlorite (Ch); R0 I-S MLM (R0 I-S); R3 I-S MLM (R3 I-S); illite/mica (I/M); illite polytype ($1M_t$); sudoite (Su); kaolinite (K)).

Although there is no clear trend between sudoite and I-S MLMs, XRD modeled data show that the increasing amount of sudoite tends to be accompanied by decreasing R0 I-S MLMs in sandstones and siltstones. Moreover, sudoite contents seem to be high with increasing kaolinite contents. Nonetheless, these correlations might be biased as little XRD profile simulations have been conducted and absence of quantitative analyses.

The chemical composition, measured by EDX, and calculated structural formulas (based on 14 oxygen equivalents and with all Fe assumed as Fe^{2+} for chlorite group minerals) are shown in Table S2. The Mg–Fe–Al_T ternary plot [Velde, 1985] shows that chlorite in the FB_{2b} black shales have a near-uniform compositions and fall between (Mg-rich chlorite) and chamosite (Fe-rich chlorite) endmembers (Figure 6a). When plotted in the trioctahedral half-vector representation of chlorite compositions [Wiewióra and Weiss, 1990], the FB_{2b} chlorites display heterogeneous composition due to their wide range of octahedral occupancy, varying from 5.25 to 5.95 atoms per half unit cells (aphuc), with a mean value of 5.58 aphuc (Figure 6b). In contrast, two distinctive chloritic minerals characterize the FB_{2a} sandstones with a compositional gap between di-trioctahedral and tri-trioctahedral chlorites (Figure 6). While one group of FB_{2a} chlorite falls in the tri-trioctahedral domain (mean octahedral occupancy near 5.65 aphuc) similar to that of the black shale facies, the octahedral occupancy of some FB_{2a} chlorite is restricted to 5 aphuc, which is consistent with that of di-trioctahedral chlorite (i.e., sudoite; Figure 6b). In addition, we observed an increase in the octahedral Al content from 2.83 to 3.25 aphuc in sudoite, which is the expected range of ideal sudoite [Bailey and Lister, 1989]. Nonetheless, the absence of quantitative data of the ferric iron content in chlorite structure may limit interpretations of the observed chemical trends (Figure 6). The data also dispersed along with the kaolinite–sudoite endmember mixing line.

4.3. *FTIR spectroscopy*

The MIR spectra of the bulk and <2 μm clay fraction in both MRS and host sediments from the FB_{2a} unit were analyzed to distinguish the kaolin polymorphs using the hydroxyl-stretching band region between 3800–3200 cm^{-1} [e.g., Balan et al., 2005]. For both lithologies (Figures 7a and 7b), the bulk spectra exhibit similar vibrational features; the broad band with complicated lineshapes in the 3550–3750 cm^{-1} region is assigned to 2:1 dioctahedral phyllosilicates including mica, illite, and I/S MLMs [Farmer, 1974, Madejová et al., 2011, Russell and Fraser, 1994] and the broad doublet at lower frequencies (3509 and 3528 cm^{-1}) diagnose the concomitant presence of sudoite [Billault et al., 2002, Madejová et al., 2011, Russell and Fraser, 1994]. The <2 μm clay fraction for both MRS and sandstone also reveals the presence of kaolinite (3620, 3561, 3668, 3696 cm^{-1}), corresponding to the four fundamental stretching vibrations of inner and inner-surface OH groups [Farmer, 1974, Madejová et al., 2011, Russell and Fraser, 1994].

5. Discussion

5.1. *Origin of sudoite*

The study of MRS and host sediment samples has highlighted that the kaolinite and sudoite are one of the dominant authigenic clayey constituents in the non-pyritized MRS and sandstones from the FB_{2a} unit. Lesser amounts of such clay minerals were observed in the siltstones, while they are almost absent in the pyritized MRS and black shales of the FB_{2b} unit. Although the illitization process was microbially enhanced in the FB_2 Member [Aubineau et al., 2019], this study reveals that the biological activity of MRS did not influence kaolinite and sudoite formations. However, the change in clay mineralogy is accompanied by a decreasing degree of fluid interaction with primary minerals, which is consistent with the reducing permeability from sandstones to black shales.

Kaolinite and/or smectite have been identified as the main precursor for the formation of sudoite due to their Al-bearing structural composition [Biernacka, 2014, Hillier et al., 2006]. Our examinations point to direct evidence of dissolution features of vermiform kaolinite crystals, leading to the assumption that kaolinite could have locally supplied most of Al for sudoite neoformation. The occurrence of mixing lines between kaolinite and sudoite supports the transformation of kaolinite to sudoite. Formation of sudoite has been previously reported to occur in Precambrian sandstones when oxidized and relatively acidic fluids from basement rocks

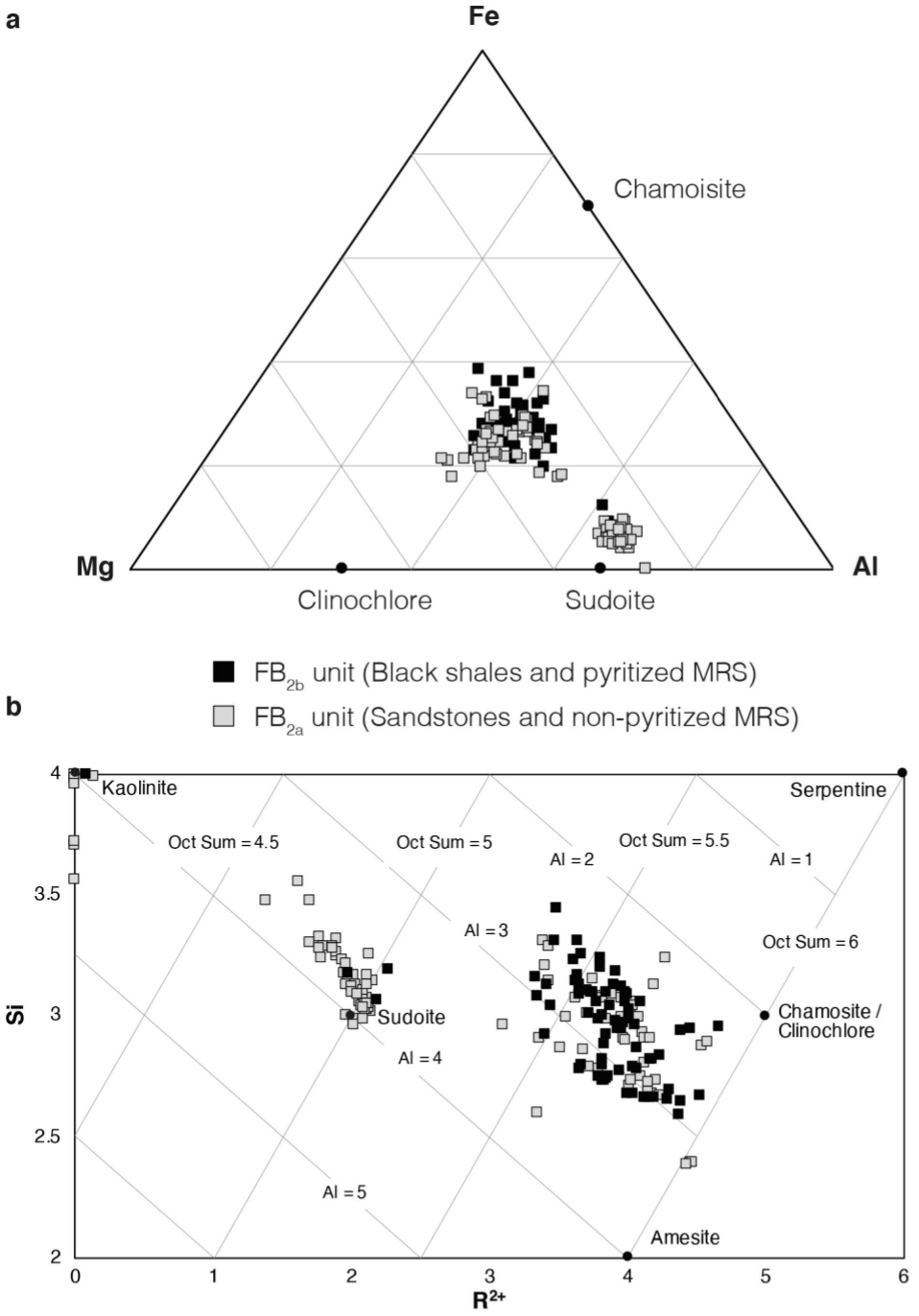

Figure 6. Projection of the structural formulas of chlorite minerals from the FB_2 Member. (a) EDX analyses of chlorite plotted in the triangular diagram Mg–Fe–Al_T [Velde, 1985]. (b) Chemical compositions of chlorite projected on the Si versus R^{2+} diagram, as designed by Wiewióra and Weiss [1990]. Data are expressed in atoms per half unit cell. The octahedral occupancy and total number of Al atoms per half unit cell are shown by contours.

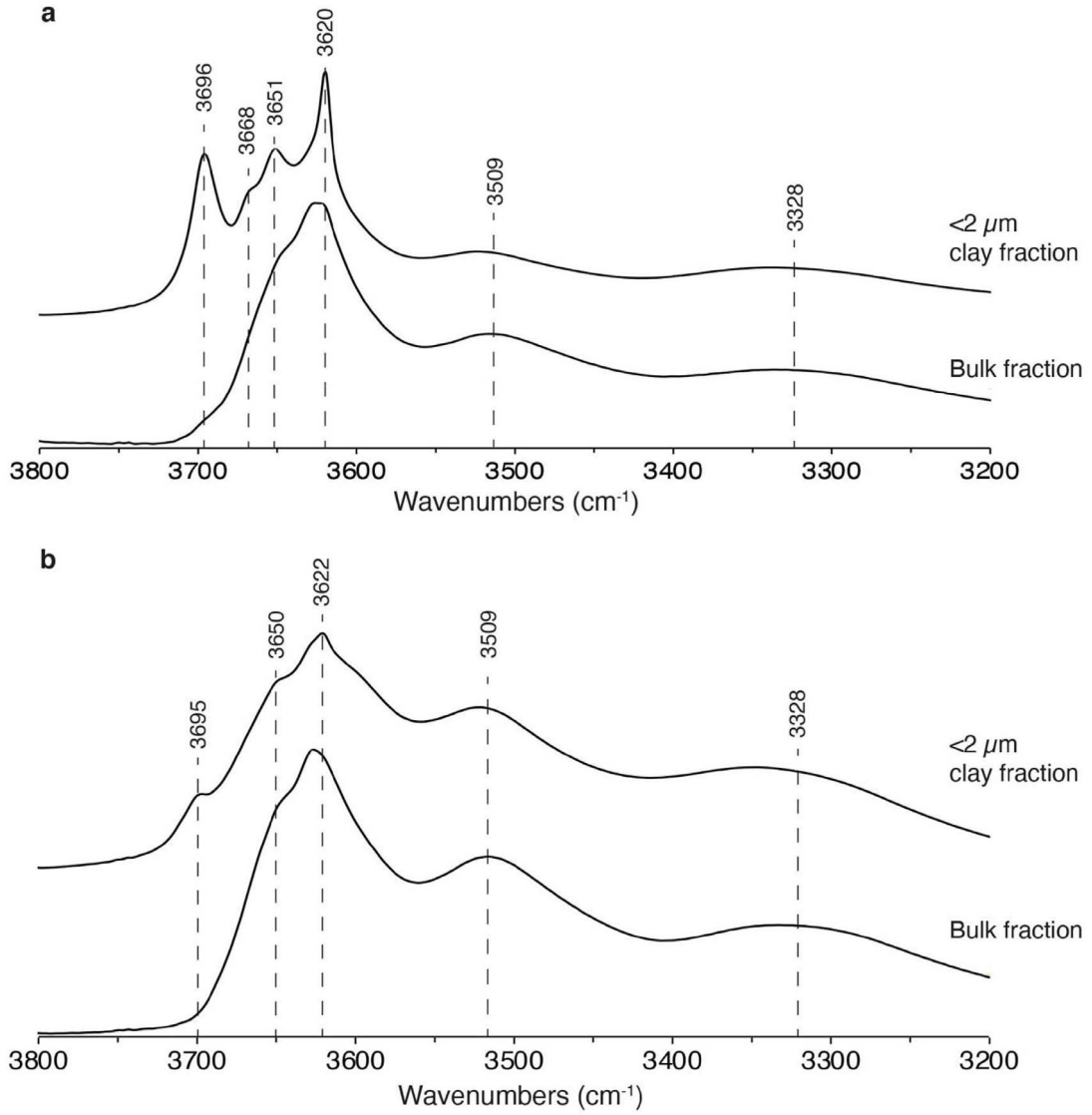

Figure 7. Typical FTIR spectra of kaolin- and sudoite-bearing samples (bulk and <2 μm clay fractions) from the FB_{2a} unit. The interval from 3800 to 3200 cm^{-1} characterizes the hydroxyl-stretching band region. (a) Mat-related structures. (b) Sandstones.

interact with overlying porous sediments [Beaufort et al., 2005, Billault et al., 2002, Riegler et al., 2014]. In addition, kaolinite–illite–sudoite paragenesis thermodynamically forms under relatively acidic and oxidizing conditions [Kister et al., 2005]. In such scenarios, circulating basinal brines along faults and fractures become saturated with respect to ions such as Fe^{2+}, Mg^{2+}, and K^{+}. The Franceville sub-basin has undergone important circulations of oxidizing basinal fluids [Bankole et al., 2016], which may be suitable for sudoite formation. Accordingly, we infer that sudoite crystallization in the FB_{2a} sandstones was promoted by fault-controlled Mg-rich brines that originated from interaction with primary minerals of the underlying Archean crystalline basement rocks. Nonetheless, we cannot completely rule out the possibility that Mg ion was supplied during the dissolution of dolomite since acidic conditions could

have destabilized Mg-bearing carbonates present in the MRS and host sediment sample.

5.2. *Mineral paragenetic sequence in the* FB_2 *Member*

Mineral paragenesis allows to unravel the relative timing of distinct diagenetic events in any sedimentary basin. The occurrence of stylolites, concavo-convex contacts between the detrital quartz grains, and closure of primary pore spaces indicate that the FB_{2a} sandstones have undergone moderate to strong degrees of compaction (Figure 2a, b). The presence of kaolinite within the secondary pore spaces and along cleavages of altered muscovite suggest their authigenic nature (Figure 2c). Kaolinization of the muscovite may have occurred at shallow burial depth during early diagenesis when the circulation of meteoritic fluids was still promoted [De Ros, 1998]. Consequently, the altered muscovite released potassium ions (K^+) into the pore system, which may have resulted in precipitation of illite within the pore space, implying that kaolinite likely predates the authigenic illite. Moreover, the occurrence of $1M_t$ illite polytype suggests environmental conditions marked by high fluid/rock ratios, while the $2M_1$ illite polytype is likely due to high burial conditions near the transition between diagenesis and metamorphism or remnants of detrital input [Meunier and Velde, 2004]. The presence of trace amounts of R0 I-S MLMs in the sandstones indicates low temperature conditions [e.g., Velde et al., 1986], supporting dominant detrital source of $2M_1$ illite phase. The progressive conversion of smectite into randomly interstratified and ordered I-S MLMs in sedimentary basins is mostly kinetic controlled, and depends on several factors including burial depth, time, temperature, pressure, primary composition, porosity, permeability, and K availability during diagenesis [Cuadros and Linares, 1996, Eberl and Hower, 1976, Howard and Roy, 1985, Hower et al., 1976, Huang et al., 1993, Inoue, 1983, Li et al., 2016, Velde et al., 1986, Whitney, 1990, among others]. In light of these considerations, the occurrence of the 2.1 Ga old R0 I-S MLMs suggests that the incomplete illitization process was not only related to insufficient K [Bankole et al., 2018, Ngombi-Pemba et al., 2014] but also to the low porosity and permeability of the FB sandstones.

The diagenetic tri-trioctahedral chlorite could have crystallized at the expense of the detrital ferromagnesian chlorite in the FB_{2a} sandstones. This is, however, unlikely due to the unaltered nature of the detrital chlorites (Figure 2d), suggesting direct precipitation of the diagenetic tri-trioctahedral chlorite from pore fluids within the pore space. This would therefore imply a higher iron content in the structural composition of authigenic chlorite relative to the detrital component [Beaufort et al., 2015]. On the other hand, our samples contain only one population of tri-trioctahedral chlorite (Figure 6), favoring the formation of the diagenetic chlorite from dissolving detrital biotite in the FB_2 Member. This inference is supported by the presence of trace amounts of titanium, released from the chloritization of biotite [Ferrow and Baginski, 1998], in the structural formulas of FB_2 tri-trioctahedral chlorite (Table S2).

The moderate to high degrees of rock compaction and occlusion of pore spaces may have limited the growth of sudoite. In addition, the small amount of octahedral iron in the structural composition of sudoite is likely responsible for the small particle size and subhedral to anhedral morphology of plates [Billault et al., 2002]. This probably explains the overall chaotic arrangement of sudoite crystals in the FB_2 Member. The presence of illite between quartz grain contacts indicates its formation or precursor before significant compaction or during compaction (syn-compaction), while the absence of chloritic minerals between quartz grain contacts suggests their formation postdates compaction. However, it is difficult to constrain the sequence of formation of the diagenetic illite and chlorite within pore space based on their textural relationships. Sudoite and illite were observed cross-cutting each other, suggesting that both minerals may have precipitated concurrently (Figure 2e–f).

5.3. *Implications for diagenetic history of the Franceville sub-basin*

While putative detrital kaolinite particles have been invoked in the overlying Francevillian sediments [Hao et al., 2021], our study reveals the presence of authigenic kaolinite in the Franceville sub-basin through a combination of petrographic, microscopic, and mineralogical analyses. Authigenic kaolin polytypes promote the investigation of burial history

of sedimentary basins since a continuous sequence of kaolinite-to-dickite transformation occurs during diagenesis [Beaufort et al., 1998, Lanson et al., 2002]. Through a dissolution–precipitation mechanism, vermicular kaolinite crystals can be progressively replaced by blocky dickite, which is the stable kaolin polymorph during late diagenesis [Zotov et al., 1998]. The main parameters controlling the reaction are the burial depth and temperature, which establishes that the first step of kaolinite–dickite transition usually takes place at burial depth about 2500 m in conditions of normal geothermal gradient. The lack of petrographic and mineralogical evidence of dickite in the FB_2 Member, therefore, suggests that the Francevillian sediments have not experienced deep burial diagenesis.

The kaolinite–illite–sudoite paragenetic sequence in the FB_2 Member can be explained by an increase of the K^+/H^+ and $Mg^{2+}/(H^+)^2$ activity ratios with a higher $Mg^{2+}/(H^+)^2$ ratio than K^+/H^+ ratio [Kister et al., 2005]. This kinetic fluid–rock reaction path predicts that kaolinite does not completely dissolve and sudoite crystallizes concomitantly with $1M_t$ illite, which is consistent with our petrographic observations. Such reaction occurs under relatively acidic and oxidizing conditions with the involvement of basinal fluids circulating along faults and fractures [Kister et al., 2005]. Through upward circulations, similar diagenetic hydrothermal brines are known to have promoted the U mobilization and its enrichment at the reduction front of the FA–FB transition in the Franceville sub-basin [Bankole et al., 2016, Gauthier-Lafaye and Weber, 1989]. These fluid circulations could have been favored by major tectonic structures during basin inversion [Gauthier-Lafaye and Weber, 1989]. Accordingly, the timing of sudoite formation in the overlying FB_2 sandstone facies could have coincided with upward migrating fluids that resulted in U mineralization during the late burial stage of the Francevillian Group. One possible assumption for the lack of sudoite in the FA sandstones would be the complete absence of kaolin minerals [Bankole et al., 2015], which contrasts with the mineralogical composition of other sandstone-hosted U deposits in the Paleoproterozoic Athabasca basin (Canada) and McArthur basin (Australia) [Beaufort et al., 2005, Billault et al., 2002, Kister et al., 2005, Percival and Kodama, 1989, Riegler et al., 2014, Truche et al., 2018].

6. Conclusion

The Paleoproterozoic FB_2 Member in the Franceville sub-basin consists of sandstones and black shales intercalated with siltstone beds that were deposited in relatively shallow environments, which triggered the development of photosynthesizing microbial mat communities [Aubineau et al., 2018, Reynaud et al., 2017].

This study documents the clay mineralogy in remnants of microbial mats and host sediments to better constrain the mineral paragenesis in the FB_2 Member. The textural relationships and mineralogical compositions of the MRS and host rocks indicate that multiple diagenetic processes affected the FB_2 Member. In addition to the FB_2 detrital clay minerals and $2M_1$ illite, as well as authigenic minerals ($1M_t$ illite, I-S MLMs, and ferromagnesian chlorite), the FB_{2a} MRS and sandstones and also FB_{2b} siltstones to a lesser extent are further characterized by vermiform kaolinite and sudoite. Specifically, the medium- to coarse-grained sediments reveal the co-occurrence of kaolinite, $1M_t$ illite, and sudoite, which supports a fault-controlled environment with a high fluid/rock ratio under acidic and oxidized condition. The absence of kaolinite and sudoite in the pyritized MRS and black shale facies highlights, thus, the role of porosity and permeability of sedimentary rocks in the clay authigenesis in the FB_2 Member.

Acknowledgments

We deeply thank the Gabonese Government, CENAREST, the General Direction of Mines and Geology, and the Agence Nationale des Parcs Nationaux of Gabon for the logistic supports. La Région Nouvelle Aquitaine, France, the European Union (ERDF), and the French Embassy in Libreville, Gabon, supported this work. We would like to acknowledge Professors P. Mouguiama Daouda, J. C. Balloche, L. White, and R. Oslisly for their support. The authors also thank C. Boissard, C. Fontaine, C. Laforest, and P. Recourt for laboratory support at the universities of Poitiers and Lille. The authors are particularly thankful to Professors A. Meunier and D. Beaufort for scientific discussions and C. Lebailly for administrative support.

Supplementary data

Supporting information for this article is available on the journal's website under https://doi.org/10.5802/crgeos.62 or from the author.

References

Aubineau, J., El Albani, A., Bekker, A., Chi Fru, E., Somogyi, A., Medjoubi, K., Riboulleau, A., Meunier, A., and Konhauser, K. O. (2020). Trace element perspective into the *ca.* 2.1-billion-year-old shallow-marine microbial mats from the Francevillian Group, Gabon. *Chem. Geol.*, 543, article no. 119620.

Aubineau, J., El Albani, A., Bekker, A., Somogyi, A., Bankole, O. M., Macchiarelli, R., Meunier, A., Riboulleau, A., Reynaud, J.-Y., and Konhauser, K. O. (2019). Microbially induced potassium enrichment in Paleoproterozoic shales and implications for reverse weathering on early Earth. *Nat. Commun.*, 10, article no. 2670.

Aubineau, J., El Albani, A., Chi Fru, E., et al. (2018). Unusual microbial mat-related structural diversity 2.1 billion years ago and implications for the Francevillian biota. *Geobiology*, 16, 476–497.

Aubineau, J., El Albani, A., Chi Fru, E., Kipp, M. A., Ngwal'ghoubou Ikouanga, J., and Bekker, A. (2021). Benthic redox conditions and nutrient dynamics in the ca. 2.1 Ga Franceville sub-basin. *Precambrian Res.*, 360, article no. 106234.

Azziley Azzibrouck, G. (1986). *Sédimentologie et géochimie du Francevillien B (protérozoïque inférieur). Métallogénie des gisements de manganèse de Moanda, Gabon.* Université Louis Pasteur, Strasbourg.

Bailey, S. W. (1980). Structure of layer silicates. In Brindley, G. W. and Brown, G., editors, *Crystal Structure of Clay Minerals and Their X-Ray Identification*, pages 1–123. Mineralogical Society, London.

Bailey, S. W. and Lister, J. S. (1989). Structures, compositions, and X-ray diffraction identification of dioctahedral chlorites. *Clays Clay Miner.*, 37, 193–202.

Balan, E., Lazzeri, M., Saitta, A. M., Allard, T., Fuchs, Y., and Mauri, F. (2005). First-principles study of OH-stretching modes in kaolinite, dickite, and nacrite. *Am. Mineral.*, 90, 50–60.

Bankole, O. M., El Albani, A., Meunier, A., and Gauthier-Lafaye, F. (2015). Textural and paleo-fluid flow control on diagenesis in the Paleoproterozoic Franceville Basin, South Eastern, Gabon. *Precambrian Res.*, 268, 115–134.

Bankole, O. M., El Albani, A., Meunier, A., Pambo, F., Paquette, J.-L., and Bekker, A. (2018). Earth's oldest preserved K-bentonites in the *ca.* 2.1 Ga Francevillian Basin, Gabon. *Am. J. Sci.*, 318, 409–434.

Bankole, O. M., El Albani, A., Meunier, A., Poujol, M., and Bekker, A. (2020). Elemental geochemistry and Nd isotope constraints on the provenance of the basal siliciclastic succession of the middle Paleoproterozoic Francevillian Group, Gabon. *Precambrian Res.*, 348, article no. 105874.

Bankole, O. M., El Albani, A., Meunier, A., Rouxel, O. J., Gauthier-Lafaye, F., and Bekker, A. (2016). Origin of red beds in the Paleoproterozoic Franceville Basin, Gabon, and implications for sandstone-hosted uranium mineralization. *Am. J. Sci.*, 316, 839–872.

Beaufort, D., Cassagnabère, A., Petit, S., Lanson, B., Berger, G., Lacharpagne, J. C., and Johansen, H. (1998). Kaolinite-to-dickite reaction in sandstone reservoirs. *Clay Miner.*, 33, 297–316.

Beaufort, D., Patrier, P., Laverret, E., Bruneton, P., and Mondy, J. (2005). Clay alteration associated with Proterozoic unconformity-type Uranium deposits in the east alligator rivers uranium field, Northern Territory, Australia. *Econ. Geol.*, 100, 515–536.

Beaufort, D., Rigault, C., Billon, S., Billault, V., Inoue, A., Inoue, S., and Patrier, P. (2015). Chlorite and chloritization processes through mixed-layer mineral series in low-temperature geological systems—a review. *Clay Miner.*, 50, 497–523.

Bertrand-Sarfati, J. and Potin, B. (1994). Microfossiliferous cherty stromatolites in the 2000 Ma Franceville group, Gabon. *Precambrian Res.*, 65, 341–356.

Biernacka, J. (2014). Pore-lining sudoite in Rotliegend sandstones from the eastern part of the Southern Permian Basin. *Clay Miner.*, 49, 635–655.

Billault, V., Beaufort, D., Patrier, P., and Petit, S. (2002). Crystal chemistry of Fe-sudoites from uranium deposits in the Athabasca basin (Saskatchwan, Canada). *Clays Clay Miner.*, 50, 70–81.

Bonhomme, M. G., Gauthier-Lafaye, F., and Weber, F. (1982). An example of Lower Proterozoic sediments: The Francevillian in Gabon. *Precambrian Res.*, 18, 87–102.

Bouton, P., Thiéblemont, D., Simo Ndounze, S., Goujou, J. C., Kassadou, A. B., Walemba, A., Boulingui, B., Ekhogha, H., Moussavou, M., Lambert, A., Roberts, D., Deschamps, Y., and Préat, A. (2009). *Carte géologique de la République du Gabon à 1/200 000, feuille Franceville - Boumango*. DGMG Editions - Ministère des Mines, du Pétrole, des Hydrocarbures, Libreville.

Brindley, G. W. and Brown, G. (1980). *Crystal Structure of Clay Minerals and their X-ray Identification*. Mineralogical Society, London.

Bros, R., Stille, P., Gauthier-Lafaye, F., Weber, F., and Clauer, N. (1992). Sm–Nd isotopic dating of Proterozoic clay material: An example from the Francevillian sedimentary series, Gabon. *Earth Planet. Sci. Lett.*, 113, 207–218.

Canfield, D. E., Ngombi-Pemba, L., Hammarlund, E. U., Bengtson, S., Chaussidon, M., Gauthier-Lafaye, F., Meunier, A., Riboulleau, A., Rollion-Bard, C., Rouxel, O., Asael, D., Pierson-Wickmann, A.-C., and El Albani, A. (2013). Oxygen dynamics in the aftermath of the Great Oxidation of Earth's atmosphere. *Proc. Natl. Acad. Sci. USA*, 110, 16736–16741.

Cuadros, J. and Linares, J. (1996). Experimental kinetic study of the smectite-to-illite transformation. *Geochim. Cosmochim. Acta*, 60, 439–453.

Daniels, E. J. and Altaner, S. P. (1990). Clay mineral authigenesis in coal and shale from the Anthracite region, Pennsylvania. *Am. Mineral.*, 75, 825–839.

De Ros, L. F. (1998). Heterogeneous generation and evolution of diagenetic quartzarenites in the Silurian-Devonian Fumas formation of the Paran Basin, southern Brazil. *Sediment. Geol.*, 116, 99–128.

Eberl, D. and Hower, J. (1976). Kinetics of illite formation. *Geol. Soc. Am. Bull.*, 87, 1326–1330.

El Albani, A., Bengtson, S., Canfield, D. E., Bekker, A., et al. (2010). Large colonial organisms with coordinated growth in oxygenated environments 2.1 Gyr ago. *Nature*, 466, 100–104.

El Albani, A., Bengtson, S., Canfield, D. E., Riboulleau, A., et al. (2014). The 2.1 Ga old Francevillian biota: Biogenicity, taphonomy and biodiversity. *PLoS ONE*, 9, article no. e99438.

El Albani, A., Mangano, M. G., Buatois, L. A., et al. (2019). Organism motility in an oxygenated shallow-marine environment 2.1 billion years ago. *Proc. Natl. Acad. Sci. USA*, 116, 3431–3436.

Farmer, V. C. (1974). *The Infrared Spectra of Minerals*. The Mineralogical Society, London.

Ferrow, E. A. and Baginski, B. (1998). Chloritisation of hornblende and biotite: a HRTEM study. *Acta Geol. Pol.*, 48, 107–113.

Feybesse, J. L., Johan, V., Triboulet, C., Guerrot, C., Mayaga-Mikolo, F., Bouchot, V., and Eko N'dong, J. (1998). The west central African belt: A model of 2.5–2.0 Ga accretion and two-phase orogenic evolution. *Precambrian Res.*, 87, 161–216.

Gauthier-Lafaye, F. (1986). *Les gisements d'uranium du Gabon et les réacteurs d'Oklo. Modèle métallogénique de gîtes à fortes teneurs du protérozoique inférieur*. Université Louis Pasteur, Strasbourg.

Gauthier-Lafaye, F. and Weber, F. (1989). The Francevillian (Lower Proterozoic) uranium ore deposits of Gabon. *Econ. Geol.*, 84, 2267–2285.

Gauthier-Lafaye, F. and Weber, F. (2003). Natural nuclear fission reactors: Time constraints for occurrence, and their relation to uranium and manganese deposits and to the evolution of the atmosphere. *Precambrian Res.*, 120, 81–100.

Hao, W., Mänd, K., Li, Y., Alessi, D. S., Somelar, P., Moussavou, M., Romashkin, A. E., Lepland, A., Kirsimäe, K., Planavsky, N. J., and Konhauser, K. O. (2021). The kaolinite shuttle links the Great Oxidation and Lomagundi events. *Nat. Commun.*, 12, article no. 2944.

Hayashi, H. and Oinuma, K. (1964). Aluminian chlorite from Kamikita mine, Japan. *Clay Sci.*, 2, 22–30.

Hillier, S., Wilson, M. J., and Merriman, R. J. (2006). Clay mineralogy of the Old Red Sandstone and Devonian sedimentary rocks of Wales, Scotland and England. *Clay Miner.*, 41, 433–471.

Horie, K., Hidaka, H., and Gauthier-Lafaye, F. (2005). U-Pb geochronology and geochemistry of zircon from the Franceville series at Bidoudouma, Gabon. In *15th Annual Goldschmidt Conference, Moscow, United States*.

Howard, J. J. and Roy, D. M. (1985). Development of layer charge and kinetics of experimental smectite alteration. *Clays Clay Miner.*, 33, 81–88.

Hower, J., Eslinger, E. V., Hower, M. E., and Perry Jr., E. A. (1976). Mechanism of burial metamorphism of argillaceous sediment: 1. Mineralogical and chemical evidence. *Geol. Soc. Am. Bull.*, 87, 725–737.

Huang, W.-L., Longo, J. M., and Pevear, D. R. (1993). An experimentally derived kinetic model for smectite-to-illite conversion and its use as a geothermometer. *Clays Clay Miner.*, 41, 162–177.

Inoue, A. (1983). Potassium fixation by clay minerals during hydrothermal treatment. *Clays Clay Miner.*, 31, 81–91.

Karhu, J. A. and Holland, H. D. (1996). Carbon isotopes and the rise of atmospheric oxygen. *Geology*, 24, 867–870.

Kister, P., Vieillard, P., Cuney, M., Quirt, D., and Laverret, E. (2005). Thermodynamic constraints on the mineralogical and fluid composition evolution in a clastic sedimentary basin: the Athabasca Basin (Saskatchewan, Canada). *Eur. J. Mineral.*, 17, 325–342.

Lanari, P., Wagner, T., and Vidal, O. (2014). A thermodynamic model for di-trioctahedral chlorite from experimental and natural data in the system MgO–FeO–Al_2O_3–SiO_2–H_2O: Applications to P–T sections and geothermometry. *Contrib. Mineral. Petrol.*, 167, article no. 968.

Lanson, B., Beaufort, D., Berger, G., Bauer, A., Cassagnabère, A., and Meunier, A. (2002). Authigenic kaolin and illitic minerals during burial diagenesis of sandstones: a review. *Clay Miner.*, 37, 1–22.

Lekele Baghekema, S. G., Lepot, K., Riboulleau, A., Fadel, A., Trentesaux, A., and El Albani, A. (2017). Nanoscale analysis of preservation of *ca.* 2.1 Ga old Francevillian microfossils, Gabon. *Precambrian Res.*, 301, 1–18.

Li, Y., Cai, J., Song, M., Ji, J., and Bao, Y. (2016). Influence of organic matter on smectite illitization: A comparison between red and dark mudstones from the Dongying Depression, China. *Am. Mineral.*, 101, 134–145.

Madejová, J., Balan, E., and Petit, S. (2011). Application of vibrational spectroscopy to the characterization of phyllosilicates and other industrial minerals. In Christidis, G. E., editor, *Advances in the Characterization of Industrial Minerals*, pages 171–226. European Mineralogical Union and Mineralogical Society of Great Britain and Ireland, Cambridge.

Meunier, A. and Velde, B. (2004). *Illite. Origins, Evolution and Metamorphism.* Springer-Verlag, Berlin, Heidelberg.

Moore, D. M. and Reynolds Jr., R. C. (1997). *X-ray Diffraction and the Identification and Analysis of Clay Minerals.* Oxford University Press, New York.

Mouélé, I. M., Dudoignon, P., El Albani, A., Meunier, A., Boulvais, P., Gauthier-Lafaye, F., Paquette, J.-L., Martin, H., and Cuney, M. (2014). 2.9–1.9 Ga paleoalterations of Archean granitic basement of the Franceville basin (Gabon). *J. African Earth Sci.*, 97, 244–260.

Ngombi-Pemba, L., El Albani, A., Meunier, A., Grauby, O., and Gauthier-Lafaye, F. (2014). From detrital heritage to diagenetic transformations, the message of clay minerals contained within shales of the Palaeoproterozoic Francevillian basin (Gabon). *Precambrian Res.*, 255, 63–76.

Ossa Ossa, F., El Albani, A., Hofmann, A., Bekker, A., Gauthier-Lafaye, F., Pambo, F., Meunier, A., Fontaine, C., Boulvais, P., Pierson-Wickmann, A.-C., Cavalazzi, B., and Macchiarelli, R. (2013). Exceptional preservation of expandable clay minerals in the *ca.* 2.1 Ga black shales of the Francevillian basin, Gabon and its implication for atmospheric oxygen accumulation. *Chem. Geol.*, 362, 181–192.

Percival, J. B. and Kodama, H. (1989). Sudoite from Cigar Lake, Saskatchewan. *Can. Mineral.*, 27, 633–641.

Pombo, F. (2004). *Conditions de formation des carbonates de manganèse protérozosoïques et analyse minéralogique et géochimique des minerais à bioxydes de manganèse associés dans le gisement de Moanda (Sud-Est, Gabon).* Université de Bourgogne, Dijon.

Préat, A., Bouton, P., Thiéblemont, D., Prian, J.-P., Ndounze, S. S., and Delpomdor, F. (2011). Paleoproterozoic high $\delta^{13}C$ dolomites from the Lastoursville and Franceville basins (SE Gabon): Stratigraphic and synsedimentary subsidence implications. *Precambrian Res.*, 189, 212–228.

Reynaud, J.-Y., Trentesaux, A., El Albani, A., Aubineau, J., Ngombi-Pemba, L., Guiyeligou, G., Bouton, P., Gauthier-Lafaye, F., and Weber, F. (2017). Depositional setting of the 2.1 Ga Francevillian macrobiota (Gabon): Rapid mud settling in a shallow basin swept by high-density sand flows. *Sedimentology*, 65, 670–701.

Reynolds Jr., R. C. and Reynolds III, R. C. (1996). NEWMOD for Windows. The Calculation of One-dimensional X-ray Diffraction Patterns of Mixed-layered Clay Minerals. 8 Brook Road, Hanover, New Hampshire.

Riegler, T., Lescuyer, J.-L., Wollenberg, P., Quirt, D., and Beaufort, D. (2014). Alteration related to uranium deposits in the Kiggavik-Andrew lake structural trend, Nunavut, Canada: new insights from petrography and clay mineralogy. *Can. Mineral.*, 52, 27–45.

Rodríguez-Ruiz, M. D., Abad, I., and Bentabol,

M. J. (2019). Permo-Triassic clastic rocks from the Ghomaride Complex and Federico units (Rif Cordillera, N Morocco): An example of diagenetic-metamorphic transition. *Minerals*, 9, article no. 738.

Ruiz Cruz, M. D. and Sanz de Galdeano, C. (2005). Compositional and structural variation of sudoite from the Betic Cordillera (Spain): a TEM/AEM study. *Clays Clay Miner.*, 53, 639–652.

Russell, J. D. and Fraser, A. R. (1994). Infrared methods. In Wilson, M. J., editor, *Clay Mineralogy: Spectroscopic and Chemical Determinative Methods*, pages 11–67. Chapman & Hall, London.

Sawaki, Y., Moussavou, M., Sato, T., Suzuki, K., Ligna, C., Asanuma, H., Sakata, S., Obayashi, H., Hirata, T., and Edou-Minko, A. (2017). Chronological constraints on the Paleoproterozoic Francevillian Group in Gabon. *Geosci. Front.*, 8, 397–407.

Schultz, L. G. (1963). *Clay Minerals in Triassic Rocks of the Colorado Plateau*. Geological Survey Bulletin 1147–C. U.S. Government Printing Office, Washington D.C.

Thiéblemont, D., Bouton, P., Préat, A., Goujou, J.-C., Tegyey, M., Weber, F., Ebang Obiang, M., Joron, J. L., and Treuil, M. (2014). Transition from alkaline to calc-alkaline volcanism during evolution of the Paleoproterozoic Francevillian basin of eastern Gabon (Western Central Africa). *J. African Earth Sci.*, 99, 215–227.

Thiéblemont, D., Castaing, C., Billa, M., Bouton, P., and Préat, A. (2009). *Notice explicative de la carte géologique et des ressources minérales de la République gabonaise à 1/1 000 000*. DGMG Editions - Ministère des Mines, du Pétrole, des Hydrocarbures, Libreville.

Truche, L., Joubert, G., Dargent, M., Martz, P., Cathelineau, M., Rigaudier, T., and Quirt, D. (2018). Clay minerals trap hydrogen in the Earth's crust: Evidence from the Cigar Lake uranium deposit, Athabasca. *Earth Planet. Sci. Lett.*, 493, 186–197.

Velde, B. (1985). *Clay Minerals: A Physico-Chemical Explanation of their Occurrence*. Elsevier, Amsterdam.

Velde, B., Suzuki, T., and Nicot, E. (1986). Pressure-temperature-composition of illite/smectite mixed-layer minerals: Niger delta mudstones and other examples. *Clays Clay Miner.*, 34, 435–441.

Weber, F. (1968). *Une série précambrienne du Gabon : le Francevillien. Sédimentologie, géochimie, relations avec les gîtes minéraux associés*. Université de Strasbourg, Strasbourg.

Weber, F., Gauthier-Lafaye, F., Whitechurch, H., Ulrich, M., and El Albani, A. (2016). The 2-Ga Eburnean Orogeny in Gabon and the opening of the Francevillian intracratonic basins: A review. *C. R. Geosci.*, 348, 572–586.

Whitney, G. (1990). Role of water in the smectite-to-illite reaction. *Clays Clay Miner.*, 38, 343–350.

Wiewióra, A. and Weiss, Z. (1990). Crystallochemical classifications of phyllosilicates based on the unified system of projection of chemical composition: II. The chlorite group. *Clay Miner.*, 25, 83–92.

Zotov, A., Mukhamet-Galeev, A., and Schott, J. (1998). An experimental study of kaolinite and dickite relative stability at 150–300 °C and the thermodynamic properties of dickite. *Am. Mineral.*, 83, 519–524.